ACS Sustainable Chemistry & Engineering

pubs.acs.org/journal/ascecg

Research Article

Particle Size Reduction of Poly(ethylene terephthalate) Increases the Rate of Enzymatic Depolymerization But Does Not Increase the Overall Conversion Extent

Richard K. Brizendine, Erika Erickson, Stefan J. Haugen, Kelsey J. Ramirez, Joel Miscall, Davinia Salvachúa, Andrew R. Pickford, Margaret J. Sobkowicz, John E. McGeehan,* and Gregg T. Beckham*

Cite This: https://doi.org/10.1021/acssuschemeng.2c01961

Read Online

ACCESS | Metrics & More | Article Recommendations | Supporting Information

ABSTRACT: Enzymatic depolymerization of poly(ethylene terephthalate) (PET) has emerged as a potential method for PET recycling, but extensive thermomechanical preprocessing to reduce both the crystallinity and particle size of PET is often conducted, which is costly and energy-intensive. In the current work, we use high-crystallinity PET (HC-PET) and low-crystallinity cryomilled PET (CM-PET) with three distinct particle size distributions to investigate the effect of PET particle size and crystallinity on the performance of a variant of the leaf compost-cutinase enzyme (LCC-ICCG). We show that LCC-ICCG hydrolyzes PET, resulting in the accumulation of terephthalic acid and, interestingly, also releases significant amount of mono(2-hydroxyethyl)terephthalate. Particle size reduction of PET increased the maximum rate of reaction for HC-PET, while the maximum hydrolysis rate for CM-PET was not significantly different across particle sizes. For both substrates, however, we show that particle size reduction has little effect on the overall conversion extent. Specifically, the CM-PET film was converted to 99 ± 0.2% mass loss within 48 h, while the HC-PET powder reached only 23.5 ± 0.0% conversion in 144 h. Overall, these results suggest that amorphization of PET is a necessary pretreatment step for enzymatic PET recycling using the LCC-ICCG enzyme but that particle size reduction may not be required.

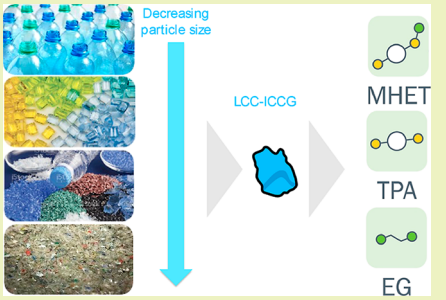

KEYWORDS: *plastic recycling, cutinase, interfacial biocatalysis, kinetics, crystallinity, particle size*

INTRODUCTION

Plastics are necessary in today's world, but most plastics are not recycled and instead are discarded in landfills or accumulate in the environment.[1−3] Poly(ethylene terephthalate) (PET), with ∼65 million metric tons produced annually,[4−6] is the second most abundantly produced plastic, behind only polyethylene. Currently, the most common type of PET recycling is thermomechanical, which often results in recycled polymers with less desirable mechanical properties than those produced from virgin terephthalic acid (TPA) and ethylene glycol,[7] which are the monomers used for PET synthesis. Therefore, chemical recycling technologies that can depolymerize PET to its constituent monomers are of keen interest to regenerate virgin-quality PET.[8]

Enzymatic recycling is an emerging chemical recycling strategy for PET due to the relatively low temperature and pressure required, as well as high selectivity in the enzymatic reactions, possibly enabling precise PET depolymerization within complex mixed waste streams that have been previously excluded from recycling processes.[9−11] Many PET-degrading enzymes have been previously reported and characterized,[12−25] but most show limited activity on PET and are therefore likely not directly suitable for industrial use. There have recently been many efforts to enhance the thermostability and catalytic activity of several PET hydrolases to this end.[26−46]

To date, some of the highest depolymerization extents of PET were reported by Tournier *et al.*[39] The authors reported an engineered variant of leaf compost-cutinase (LCC)[17,19] capable of degrading PET to >90% within 10 h. While the authors concluded that this performance is sufficient for industrial-scale recycling, the PET used in their study was extensively preprocessed to reduce long-range order and crystallinity (amorphization) and reduce particle size (micronization) prior to enzymatic degradation. These are fundamental process parameters, given that techno-economic analysis (TEA) suggests that mechanical preprocessing of PET is a main contributor to cost, energy consumption, and greenhouse gas emissions of the process.[47] Specifically, the analysis suggests that by eliminating mechanical pretreatment, the

Received: April 4, 2022
Revised: June 22, 2022

process electricity usage decreases by 67%, the overall process energy reduces by almost 50%, and the minimum selling price of the recovered TPA is reduced by $0.24/kg.[47] However, to our knowledge, little work has been reported on the effect of amorphization and micronization of PET with these recently developed enzymes. It is well accepted that many reported PET-hydrolyzing enzymes work better on amorphous PET,[15,38,48] with *Ideonella sakaiensis* PETase (*Is*PETase) and several recently reported variants thereof being possible exceptions.[22,34,40,49−51] Moreover, studies from Castro *et al.* and Gamerith *et al.* have shown that reducing the PET particle size increased the conversion rate and the overall extent of conversion;[52−54] however, the enzymes used have not been reported to achieve the same conversion extents as the current engineered LCC variant.[39]

In this study, we investigated the effect of particle size reduction and crystallinity on the performance of PET depolymerization by the LCC-ICCG variant.[39] We prepared PET particles with low and high crystallinities across three particle size ranges each, and the PET hydrolysis performance of LCC-ICCG was tested on these substrates at varying solid and enzyme loadings. We used the inverse Michaelis−Menten (invMM) analysis proposed by Westh *et al.* to compare the enzyme kinetics across the PET substrates.[55−57] Additionally, we performed reactions in bioreactors to investigate the enzyme performance in a pH-controlled environment. Our results suggest that decreasing the particle size of PET increases the initial rate of the reaction but has little effect on the overall conversion extent. Instead, the results show that crystallinity of the PET substrate is the key driver of enzymatic PET degradation with this enzyme system.

MATERIALS AND METHODS

Reagents, Stocks, and Buffers. All chemicals were obtained from Sigma-Aldrich at the highest available grade of purity and used as supplied, unless otherwise noted. Buffers were made using ultrapure water. Equilibration buffer: 20 mM Tris, pH 8, 300 mM NaCl, and 10 mM imidazole. Elution buffer: 20 mM Tris, pH 8, 300 mM NaCl, and 500 mM imidazole. Assay buffer: 100 mM NaPi, pH 8.

Preparation and Characterization of PET Particles. Amorphous PET particles (which we denote CM-PET) were prepared by cryomilling a 0.25 mm thick amorphous PET film (A-PET, Goodfellow, ES301445). The film was cut into squares with 0.5 × 0.5 cm dimensions and cryomilled in 1−2 g aliquots in stainless-steel vials using a Freezer Mill 6770 (Spex SamplePrep) and ground for a total of 40 min using the following grinding cycle: 4 min grinding, 2 min cooling, with 10 cycles in total. High-crystallinity PET particles (denoted HC-PET) were sourced from Goodfellow (ES306031).

To separate the particles by size, the PET particles were wet sieved using two sieve sizes: 250 and 125 μm sieves (Prüfsieb). Briefly, 5−10 g of PET powder was placed in the 250 μm sieve and ddH_2O was slowly run over the top. The filtrate was collected until no PET was observed in the water (usually 8−10 L). This process was repeated with the 125 μm sieve. The PET that went through the 125 μm sieve was collected by filtering the solution using Whatman grade 5 filter paper (Cytiva) and a Büchner funnel. The PET remaining in the 250 μm sieve was termed the "250 μm fraction", the PET remaining in the 125 μm sieve was similarly termed the "125 μm fraction", and the PET that went through the 125 μm sieve was denoted as the "sub125 μm fraction". All PET particles were dried at 40 °C for 2 days under vacuum.

The particle size distributions of each sieve fraction were determined using dark-field stereomicroscopy. PET particles were suspended in 1% (w/v) sodium dodecyl sulfate and spread over a glass slide (Fisher Scientific) at a concentration that reduced contact between individual particles (~500 μg mL^{-1}). The 250 and 125 μm sieve fractions were imaged at 2× magnification, and the sub125 μm sieve fraction was imaged at 4× magnification on a Nikon SMZ1500 stereomicroscope equipped with a Nikon Ds-Fi1 camera. Particle sizes were obtained by analysis with a custom ImageJ macro (NIH). Briefly, individual particles were segmented by making the image binary and using Analyze Particles function. Particles were fit to an ellipse, and the surface area and volume were estimated by assuming the height of the particle was the average of the short and long axes of the ellipse. The mass of the particles was estimated using the density of PET, 1.38 g cm^{-3}. The specific surface area was then calculated as the estimated sum of surface area over the sum of the mass of all analyzed particles.

Detailed imaging of individual PET particles was performed on a Nikon Eclipse E800 using either 10× 0.45 NA or 20× 0.75 NA PlanApo Nikon objectives, dark-field illumination, and a SPOT RTKE CCD camera (Diagnostic Instruments). PET particles were sprinkled onto a glass slide and distributed to isolate the particles. Image slices were collected at varying depths of field by manually changing the focus from the slide surface to the top of the particle and capturing images every ~2−5 μm. The images were stacked using the Focus Merge function in Affinity Photo (Serif).

The crystallinity of all PET substrates was determined by differential scanning calorimetry (DSC) using a Q2000 DSC (TA Instruments) on 2−8 mg of PET samples placed in hermetically sealed aluminum pans. The samples were analyzed from 0 to 300 °C at a rate of 10 °C min^{-1}. The glass-transition temperature (T_g), heat of melting (ΔH_m), and heat of cold crystallization (ΔH_{cc}) were determined with Universal Analysis (TA Instruments). Percent crystallinity was calculated using the following equation, where ΔH_m° is the reference heat of melting for PET = 140.1 J g^{-1}

$$\% \text{ crystallinity} = [\Delta H_m - \Delta H_{cc}]/\Delta H_m^\circ \times 100\% \quad (1)$$

The weight-average molar mass (M_w) and number-average molar mass (M_n) were determined by gel permeation chromatography (GPC) using an Agilent 1260 Infinity II LC system, which consisted of a 1260 Iso pump module, 1260 vial sampler module, and a 1260 Multicolumn Thermosat module. Three PL HFIPgel 250 × 4.6 mm columns (Agilent, PL1514-5900HFIP) attached in series were used for analysis, with a matching guard column attached. Samples were prepared in 0.22 μm filtered hexafluoroisopropanol (HFIP) at a concentration of 2 mg mL^{-1} and filtered through a 0.22 μm filter. The operating conditions included HFIP as the carrier solvent, a flow rate of 0.4 mL min^{-1}, column temperature set to 40 °C, and a sample injection of 100 μL. Detectors consisted of a miniDAWN TREOS multiangle light-scattering detector (Wyatt Technology) used in combination with an Optilab T-rEX refractive index detector (Wyatt Technology). Wyatt Technologies Astra 7.2 software was used to analyze the data.

Expression and Purification of the LCC-ICCG Enzyme. The LCC-ICCG enzyme was expressed and purified similar to the method reported by Tournier *et al.*[39] The LCC-ICCG DNA was synthesized (Twist Bioscience) and cloned into pET-21b(+) (EMD Biosciences). The plasmid was then transformed into OverExpress *Escherichia coli* C41 (DE3) (Lucigen) cells according to the manufacturer's protocol, plated on lysogeny broth (LB)-agar plates containing 100 μg mL^{-1} ampicillin (Amp), and incubated at 37 °C overnight. Single colonies from transformation were inoculated into a starter culture of LB liquid media containing 100 μg mL^{-1} Amp and grown at 37 °C with shaking at 250 rpm overnight. The starter culture was inoculated at a 100-fold dilution in 2× YT media (10 g of yeast extract, 16 g of tryptone, and 10 g of NaCl per 1 L media) containing 100 μg mL^{-1} Amp and grown at 37 °C to OD_{600} = 0.6−0.8. Protein expression was induced by the addition of isopropyl β-D-1-thiogalactopyranoside (IPTG) to a final concentration of 1 mM. Cells were maintained at 20 °C and 225 rpm for 18−24 h following IPTG induction, harvested by centrifugation, and stored at −80 °C until purification. Harvested cells were resuspended in lysis buffer containing 1 mg mL^{-1} lysozyme and 50 μg mL^{-1} DNAase and incubated on ice for 10 min. Cells were homogenized on ice using a sonicator (QSonica Q700) set to 50% amplitude in 10 s bursts, followed by 15−20 s cooling breaks. Total

https://doi.org/10.1021/acssuschemeng.2c01961
ACS Sustainable Chem. Eng. XXXX, XXX, XXX−XXX

sonication time was 2 min. The lysate was clarified by centrifugation at 40,000*g* for 40 min at 4 °C. Clarified lysate was then applied to a 5 or 25 mL HisTrap HP (Cytiva) column using an ÄKTA Pure chromatography system (Cytiva) and eluted with elution buffer over a 2 CV gradient. Fractions containing the protein were dialyzed overnight against 20 mM Tris, pH 8, 300 mM NaCl at room temperature. The sample was then clarified by filtration through a 0.45 μm polyvinylidene fluoride syringe filter (Thermo Scientific). The protein was then further purified by size-exclusion chromatography with HiLoad 16/60 Superdex 75 pg column (Cytiva). The enzyme could also be stored for several days at 4 °C, which caused most remaining impurities to precipitate, which were then removed by centrifugation or filtration. The enzyme was stored for up to 6 months at 4 °C with no detectable loss in activity.

Enzymatic Hydrolysis Experiments. Small-scale 1.5 mL volume reactions were performed in triplicate in 2 mL polypropylene Eppendorf tubes containing assay buffer and varying masses of PET substrate (0.5−10 mg mL^{-1}). Reaction tubes were equilibrated to 65 °C in a heat block (Thermo Scientific) for 10 min, and the reaction was started by the addition of varying concentrations of LCC-ICCG (30 nM to 5 μM final). Controls were performed with no added enzyme. Timepoints of 125 μL were removed with rapid pipetting to suspend the PET powder and immediately quenched into an equal volume of methanol. Samples were filtered through a 96-well, 0.25 μm filter plate (EMD Millipore, MSGVN22) using a vacuum manifold (Pall, 5017) into a 300 μL collection plate (Agilent, 5043-9312) and sealed with a silicone mat (Agilent, 5043-9317).

Large-scale reactions were performed at 1 L scale in duplicate in 3 L glass bioreactors (Applikon Biotechnology), which included two Rushton impellers in the stirrer shaft below the 1 L line. The gas-sparging arm and baffles were removed. Three different substrates were used: A-PET (Goodfellow, ES301445) cut into ∼1 × 1 cm squares, HC-PET that had not been separated by sieving (Goodfellow, ES306031), and residual PET fines from a bottle-to-bottle recycling plant kindly provided by Western Container Corporation (WC-PET). Briefly, 100 g of PET substrate (73 mL volume based on density of PET) was added to 893 mL of assay buffer and equilibrated to 65 °C with stirring at 250 rpm. The reaction was initiated by the addition of 35 mL of 8.6 mg mL^{-1} LCC-ICCG for a final enzyme loading of 3 mg g^{-1} PET (10.5 μM LCC-ICCG). No-enzyme controls were performed in 250 mL of assay buffer with 25 g of PET substrate in 250 mL glass jars (Corning), maintained at 65 °C in a MaxQ 6000 shaking incubator (Thermo Scientific) set at 250 rpm. Reactions proceeded for 144 h and were maintained at pH 8 with 4 N NaOH addition using a peristaltic pump controlled by an in-control module (Applikon Biotechnology). Control reactions did not require pH control since abiotic PET hydrolysis was very low or undetectable. Sample volumes of 1 mL were removed at designated time points, quenched, stored, and filtered as described above for the small-scale reactions. At the end of the reaction, the remaining A-PET was collected by filtration through Whatman grade 2 filter paper (Cytiva) and a Büchner funnel, while the remaining HC-PET and WC-PET were collected by filtration through 0.45 μm jar-top filter units (Thermo Scientific, 169-0045). The filters were preweighed, and after the PET was collected, the filters with PET were dried for 3 days at 50 °C under vacuum before the final mass of residual PET was calculated.

Ultrahigh-Performance Liquid Chromatography Analysis of Reaction Timepoints. Standards of bis(2-hydroxyethyl)-terephthalate (BHET) and TPA were acquired from Sigma-Aldrich. Mono(2-hydroxyethyl)terephthalate (MHET) was prepared as described previously.[49] Quantitation of BHET, MHET, and TPA was performed using ultra-high-performance liquid chromatography on an Infinity II 1290 system (Agilent Technologies), as described previously.[58]

Determination of Initial Rates and Kinetic Analysis. Initial rates of the reactions were determined by linear fits to the sum of the monomers released for each timepoint up to the first 5 h of the reaction. The invMM equation was used as described previously.[57] All linear and invMM fits were performed with Origin Pro 2021 (OriginLab Corporation). MHET autohydrolysis rates were fit to a single-step rate equation using KinTek Explorer (KinTek Corporation).

RESULTS AND DISCUSSION

Characterization of PET Substrates. Figure 1 shows particle size distributions of sieved PET substrates. The CM-PET particle (Figure 1A−C) size distributions are overall very similar to the HC-PET size distributions (Figure 1D,E), resulting in similar specific surface areas across the three sieve fractions and substrates (Table 1). Despite similar particle size distributions, the two sets of particle preparations exhibit different morphologies when examined with dark-field microscopy. The CM-PET particles display a variety of morphologies, including particles that appear shredded or torn (Figure S1A,C) and others that appear to be uniform, solid particles (Figure S1B). In contrast, the HC-PET particles are generally more consistently solid particles (Figure S1D−F). Interestingly, many of the HC-PET particles also exhibit complex morphological traits, including long offshoots from the main body of the particle (Figure S1D,E).

There are also substantial differences in the crystallinity of these two PET substrates. While the CM-PET particles originated from the LC-PET film (∼4% crystallinity, Table 1), the cryomilling process had a measurable effect on the crystallinity of the resulting particles since the crystallinity of the PET after cryomilling was higher than that of the starting material (Table 1 and Figure S2). Since the PET was ground at cryogenic temperatures, this increase is likely not due to heat-induced crystallization but instead could be attributed to stress-induced crystallization.[59−62] Some variation in the crystallinity of the sieve fractions was observed, with all samples having crystallinity between 7 and 15% (Table 1). A possible explanation for the variability could be artifacts of the DSC measurement, which can be variable and can tend to overestimate the crystallinity of amorphous PET.[63] Cryomilling of the PET film did not significantly alter the molecular-weight distributions as all three sieve fractions were similar to the starting material (Table 1). The HC-PET particles exhibit much higher crystallinity than the CM-PET and were more consistent across the sieve fractions, with all of them in the 32.5−35.7% crystallinity range (Table 1 and Figure S3). There was also no difference in the molecular weight distributions across the sieve fractions of the HC-PET particles (Table 1).

Effect of Particle Size and Crystallinity on Enzymatic Degradation of PET. To determine the effect of particle size on enzymatic degradation of PET, reactions were performed with different PET substrates. Figure 2, Dataset S1 shows representative time courses from small-scale depolymerization experiments conducted with 10 mg mL^{-1} PET and 1 μM LCC-ICCG. For the CM-PET (Figure 2A−C), the primary monomers released were TPA and MHET, with the MHET eventually converting to TPA over the course of the reaction. The monomer concentration eventually reached ∼70 mM. The HC-PET generally followed the same trend; however, the concentration of the monomers was overall much lower, reaching only ∼20−30 mM after 72 h (Figure 2D−F). Interestingly, for both the CM-PET and HC-PET particles, the MHET concentration appeared to be affected by the size of the particles. MHET reached the highest concentrations in the reactions with the sub125 μm PET particles for both the CM-PET and HC-PET particles.

https://doi.org/10.1021/acssuschemeng.2c01961
ACS Sustainable Chem. Eng. XXXX, XXX, XXX−XXX

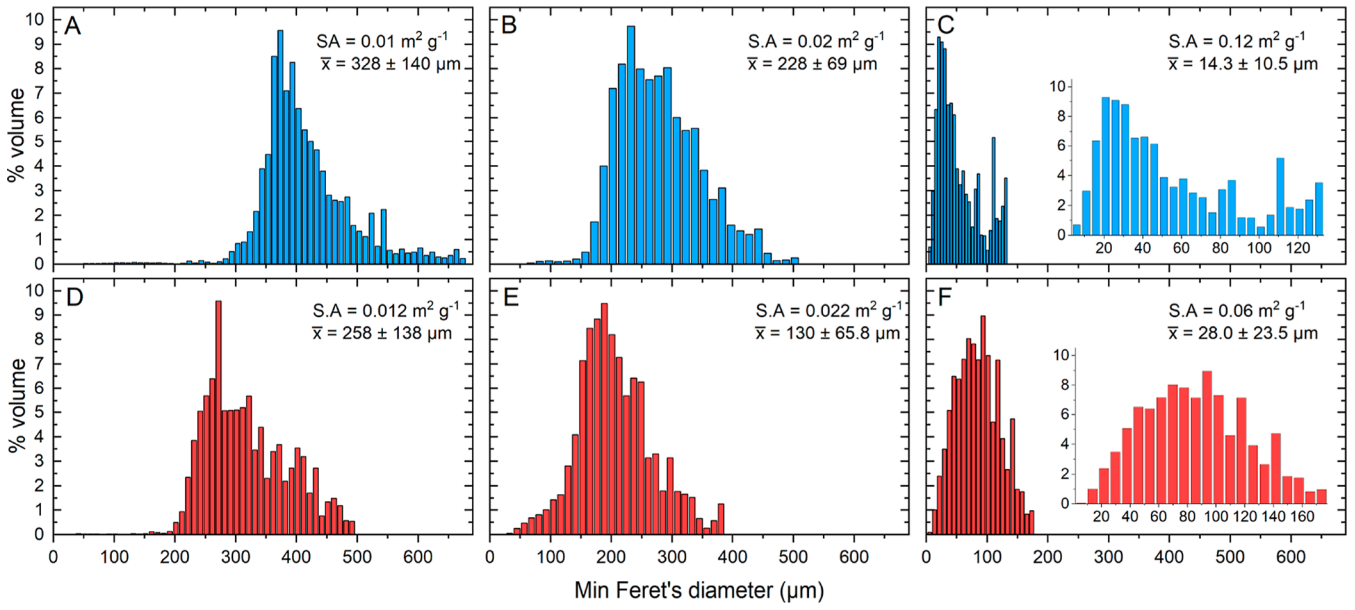

Figure 1. Size distributions of CM-PET and HC-PET particles. Histograms indicate the volume percentage as a function of Feret's minimum diameter of CM-PET (blue) and HC-PET (red) substrates. (A,D) 250, (B,E) 125, and (C,F) sub125 μm sieve fractions. Inset graphs show the expanded view of the data.

Table 1. Characterization of PET Substrates[a]

PET substrate	source	sieve fraction (μm)	specific SA ($m^2\ g^{-1}$)	T_g (°C)	% crystallinity	M_n (kDa)	M_w (kDa)
LC-PET	low-crystallinity PET film, Goodfellow ES301445	N/A	N/A	75.7 ± 0.6	4.2 ± 2	19.7 ± 8.3	33.8 ± 6.8
CM-PET	cryomilled LC-PET, from Goodfellow ES301445	250	0.01	79.0 ± 0.8	11.0 ± 1.8	20.9 ± 7.5	34.9 ± 6.7
		125	0.02	74.2 ± 0.3	7.6 ± 1	19.3 ± 8.6	34.8 ± 6.5
		sub125	0.12	69.4 ± 0.7	14.3 ± 2.3	20.3 ± 4.9	34.5 ± 6.4
HC-PET	semicrystalline powder, Goodfellow ES306031	250	0.012	76.1 ± 0.3	35.7 ± 3.8	19.9 ± 6.4	32.5 ± 7.1
		125	0.022	76.6 ± 0.6	33.0 ± 2.1	19.2 ± 5.7	33.0 ± 6.3
		sub125	0.06	76.8 ± 0.6	32.5 ± 1.7	20.1 ± 7.2	32.1 ± 6.9
WC-PET	fines supplied by Western Container Corporation	N/A	N/A	70.0 ± 0.5	37.3 ± 2.5	26.7 ± 8.4	43.5 ± 6.6

[a]Specific surface area calculated from stereomicroscopy, DSC data, and GPC data for all PET substrates. ± indicates SD, n = 3.

To examine the transient nature of MHET accumulation under these reaction conditions, we evaluated whether LCC-ICCG could catalyze MHET hydrolysis. Incubation with MHET and LCC-ICCG showed that the enzyme did not hydrolyze the substrate faster than a control reaction with no enzyme (Figure S4, Dataset S2). However, MHET spontaneously hydrolyzes under these conditions at a rate of 0.082 h^{-1} (Figure S4). This result indicates that LCC-ICCG can convert PET to both MHET and TPA and that the MHET slowly hydrolyzes to TPA explaining the transient accumulation of MHET in the reactions with PET.

To determine the effect of enzyme concentration on overall performance, we repeated the experiments shown in Figure 2 at varying enzyme concentrations (from 0.03 to 1.0 μM) and compared the concentration of monomers released after 72 h. Figure 3, Dataset S3 shows the results of these experiments. Generally, the highest extents of conversion were reached at the highest enzyme concentrations for both CM-PET and HC-PET, with very little overall difference observed between the different particle sizes. The CM-PET reached total monomer concentrations of ~70−80 mM, while the HC-PET product yields were ~3-fold lower at ~20−30 mM.

To further examine how particle size and crystallinity affect the initial rate and overall performance of the LCC-ICCG enzyme, we followed the approach described by Bååth *et al.*[57] In this approach, two different experiments are conducted: one where the PET loadings are varied with a constant enzyme concentration [conventional Michaelis−Menten (MM) approach] and one where the enzyme concentration is varied while holding the PET loading constant (invMM approach).[15,55,64] Analysis of these two experiments can provide insights into numbers of available binding sites for the enzyme on the PET surface as well as conventional specificity constants. Unfortunately, at the low enzyme concentrations and PET loadings required for conventional MM kinetics, the reaction profiles were not linear. Instead, there was a significant lag (Figure S5, Dataset S4), which makes determining the initial rates challenging and likely inaccurate. Thus, we only report the results of invMM analysis here.

Figure 4, Dataset S5 shows the invMM analysis[55,56] for the enzymatic hydrolysis of CM-PET (Figure 4A) and HC-PET particles (Figure 4B). The parameters resulting from the fits of the invMM equation to the data are shown in Table 2. The CM-PET particles exhibit similar $^{inv}K_m$ values and nearly

https://doi.org/10.1021/acssuschemeng.2c01961
ACS Sustainable Chem. Eng. XXXX, XXX, XXX−XXX

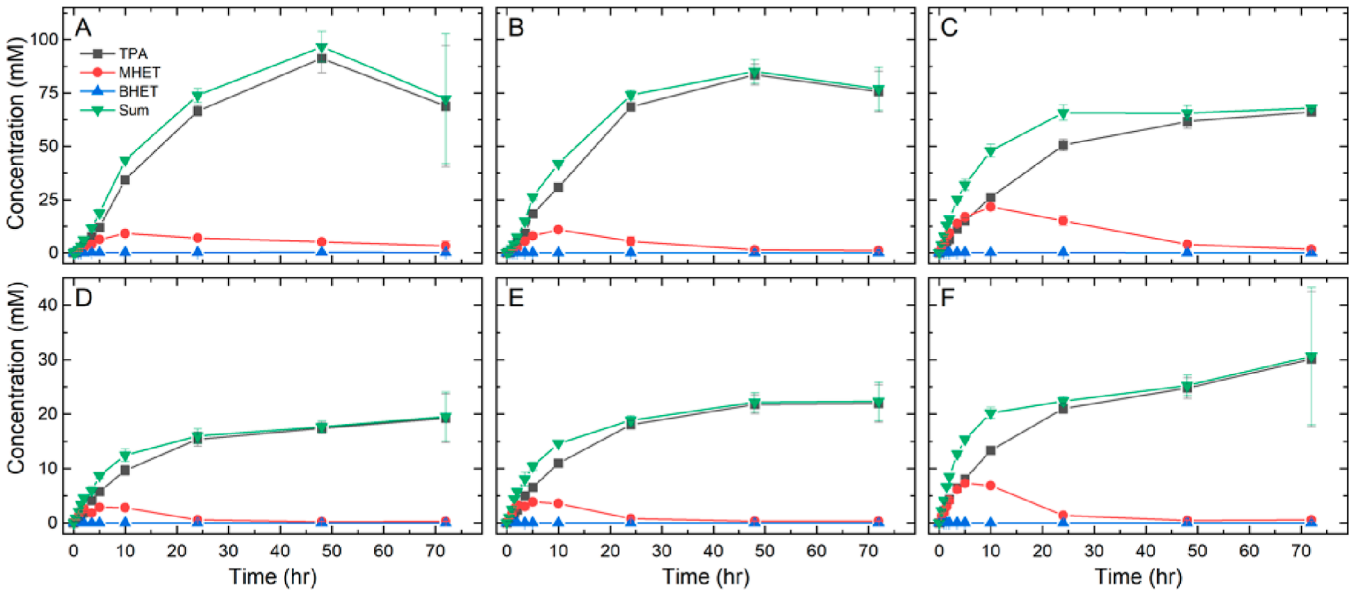

Figure 2. Monomer release as a function of time for 10 mg mL^{-1} PET particles with 1 μM LCC-ICCG. Monomers present in the reaction were analyzed by HPLC. (A) 250 μm CM-PET, (B) 125 μm CM-PET, (C) sub125 μm CM-PET, (D) 250 μm HC-PET, (E) 125 μm HC-PET, and (F) sub125 μm HC-PET. Reactions were performed in triplicate and errors bars represent the standard deviation. The data shown in this figure are provided in Dataset S1.

identical $^{inv}V_{max}$. The largest difference between the small and large particles was observed in the HC-PET, with the sub125 μm particles reaching a $^{inv}V_{max}$ approximately double that of the 250 μm sieve fraction. Generally, the smaller particle sizes resulted in higher initial rates than the larger particles. However, for the CM-PET particles, as the enzyme concentration increases, the rate of the reaction for all particles converges, whereas for the HC-PET, the initial rates were still notably different even at the high enzyme concentrations.

We also investigated the effect of PET particle size and crystallinity in 1 L scale reactions with pH control, shown in Figure 5, Dataset S6. We tested three different PET substrates: (1) A-PET cut into ~1 × 1 cm squares (Figure 5A,D), (2) HC-PET (Figure 5B,E), and (3) WC-PET (Figure 5C,F). The A-PET cut into ~1 × 1 cm squares performed the best, reaching 99 ± 0.3% conversion by mass loss and 91.3 ± 1.8% measured by HPLC analysis after ~48 h (Figure 5D). In contrast, the higher-crystallinity powders HC-PET and WC-PET reached much lower conversion extents, only reaching 23.5 ± 0.0 and 24.6 ± 0.8% degradation by mass loss, respectively, and 19.2 ± 0.9 and 24.0 ± 0.1% as measured by HPLC after 144 h (Figure 5E,F). Note the error for these numbers is the absolute difference between duplicate experiments.

Generally, the monomer release profiles from the 1 L scale reactions were similar to those from the small-scale reactions. TPA was the primary product released over time for all substrates with MHET released in a similarly transient manner as the small-scale reactions. The MHET reached similar concentrations (~10−12 mM) for all substrates tested in the bioreactors. Similarly, the LC-PET substrate (LC-PET, Figure 5A) generated significantly higher overall concentrations of monomers upon enzyme treatment, ~450 mM, when compared to the higher-crystallinity HC-PET (Figure 5B) and WC-PET (Figure 5C), which each released ~100−120 mM total monomers.

The goal of this study was to investigate the effect of PET particle size and crystallinity on the enzymatic degradation of PET with LCC-ICCG. To that end, we generated PET particles with similar sizes and surface areas but with low and high crystallinity (Figure 1 and Table 1). In small-scale tests, we observed that the sub125 μm sieve fraction particles generally achieved the highest extents of conversion during the initial 2−5 h of the reaction, suggesting that reducing the particle size has the largest effect on initial reaction rates (Figure 2). Interestingly, this observation did not necessarily translate to increased overall conversion extents since all particle sizes of a given PET substrate generally reached the same extent of conversion by the end of the reaction (Figure 3). Instead, crystallinity of the substrate appears to be the main driver for overall performance since the CM-PET (7−15% crystallinity) reached ~3-fold higher conversion extents than the HC-PET (33−35% crystallinity). These data are consistent with previous studies using various PET hydrolase enzymes and PET substrates, which also show that as the crystallinity of the PET substrate increases, the degradation performance decreases.[15,38,48] These results highlight the need for enzymes that work well on high-crystallinity PET to reduce the necessity of costly and energy-intensive pretreatment.[4,50]

While overall depolymerization extent appeared to be largely unaffected by reducing the particle size of the PET, the initial rate of the reaction was affected. We investigated this by varying the enzyme concentration with the PET particle solid loading held constant at 10 mg mL^{-1} and using an invMM analysis (Figure 4). The results of this experiment were notably different between the two different PET crystallinities. First, the HC-PET particles across all size fractions had a lower $^{inv}V_{max}$ than the corresponding CM-PET particles (Table 2). Second, comparing across the various particle sizes for each substrate, we found that the HC-PET particles with the smallest size uniformly exhibited the highest initial rate. This was not true for the CM-PET where the rates eventually converged with higher enzyme concentrations. If we assume

https://doi.org/10.1021/acssuschemeng.2c01961
ACS Sustainable Chem. Eng. XXXX, XXX, XXX−XXX

that $^{inv}V_{max}$ is governed by k_{cat},[57] then these data suggest that similar amounts of enzyme can bind to the various particle sizes of the CM-PET, resulting in similar maximal rates. However, for the HC-PET, the $^{inv}V_{max}$ is higher for the sub125 μm sieve fraction particles. This suggests that more enzymes can bind to the smaller particles, which is expected since the surface area is higher at a given solid loading. A possible explanation for this difference between the two substrates could be explained by the difference in observed morphologies for each particle preparation. The shredded appearance of the CM-PET likely made an exact measurement of surface area inaccurate, so it is possible that all sieve fractions had much larger surface areas than we estimated. This could explain why the measured $^{inv}V_{max}$ is the same for the CM-PET. Despite this, for both PET particle preparations, these results suggest that decreasing particle size or adding more enzyme can increase the initial reaction rate to a certain extent. It is important to note that this increase in initial rate did not necessarily translate to an increase in overall conversion extent, as mentioned above (Figure 3).

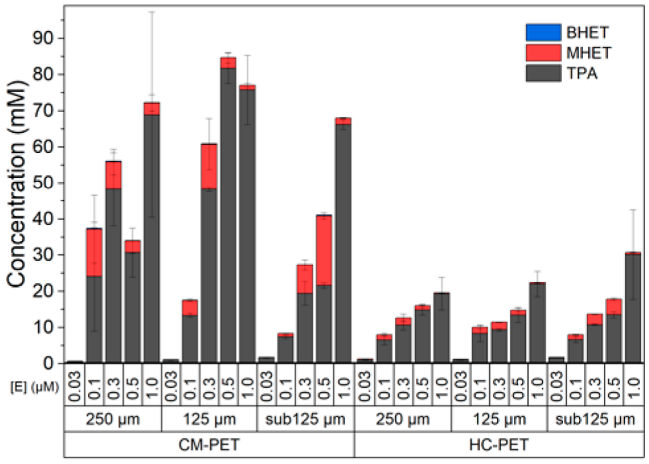

Figure 3. Total amount of monomers released from PET particles hydrolyzed with LCC-ICCG. The bars show the concentrations of all monomers released at the 72 h endpoint of the reaction with indicated [LCC-ICCG] and 10 mg mL^{-1} PET substrate. Reactions were performed in triplicate, and error bars represent standard deviation. The data shown in this figure are provided in Dataset S3.

Since it is known that the optimal pH for LCC-ICCG is ~8,[17,39] we also evaluated the effect of PET particle size and crystallinity on the performance of LCC-ICCG in bioreactors with pH control. This negates the reduction in enzyme performance due to acidification from the release of the acidic monomers. As reported previously, LCC-ICCG is capable of converting 200 g L^{-1} amorphized and micronized PET to ~90% over 10 h when incubated at 72 °C with 3 mg enzyme g PET^{-1}.[39] Figure 5A shows a similar experiment under slightly different conditions, in this case 65 °C and 100 g L^{-1} PET. A key difference is that the PET was not micronized in this experiment, instead the LC-PET film was cut into ~1 × 1 cm squares. Using the same enzyme loading of 3 mg g^{-1} PET, the reaction still reached similar conversion extent in ~48 h. We also noted a significant lag for the 1 × 1 cm squares which was not observed by Tournier *et al.* The lag seems to be dependent on surface area and enzyme concentration since a similar lag was observed in the small-scale experiments at low enzyme concentrations and low-surface-area PET particles (Figure S5).

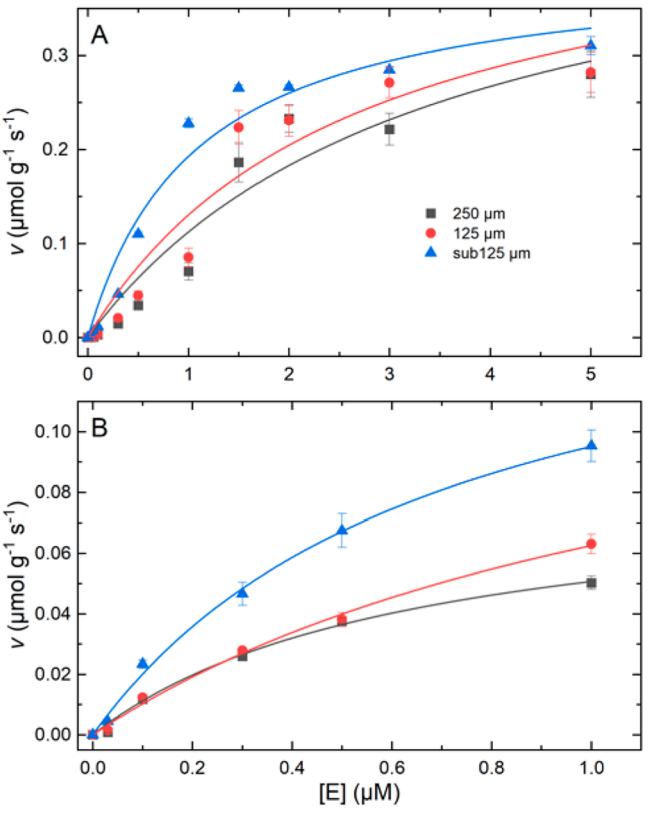

Figure 4. InvMM kinetic analysis and total amount of monomers released from PET particles upon hydrolysis with LCC-ICCG. InvMM analysis of 10 mg mL^{-1} (A) CM-PET and (B) HC-PET hydrolysis rate as a function of LCC-ICCG concentration ([E]). Lines are fits of the invMM equation. Table 2 shows the fitted parameters. Reactions were performed in triplicate and error bars represent standard deviation. The data in this figure are provided in Dataset S5.

Table 2. Kinetic Parameters from InvMM Analysis[a]

PET substrate	sieve fraction (μm)	$^{inv}K_m$ (μM)	$^{inv}V_{max}$ (μmol g^{-1} s^{-1})
CM-PET	250	3.4 ± 1.7	0.49 ± 0.14
	125	2.7 ± 1.2	0.48 ± 0.11
	sub125	1.1 ± 0.3	0.40 ± 0.04
HC-PET	250	0.6 ± 0.1	0.08 ± 0.01
	125	1.3 ± 0.3	0.14 ± 0.02
	sub125	0.7 ± 0.1	0.16 ± 0.01

[a]Calculated from data shown in Figure 3. The error indicates the standard error of the fit.

While the cause of this induction phase remains unclear, one possible explanation is the enzyme cleaves the PET polymer chains in an internal (endo) manner, as suggested in a previous study investigating the effect of crystallinity on the performance of LCC-ICCG.[65] This would not release monomers in the initial part of the reaction.

There were some interesting differences between the large- and small-scale reactions in the observed MHET concentrations. The large-scale reactions generally built up less MHET, reaching ~10−12 mM, while the MHET in the small-scale reactions could reach up to ~21 mM (Figure 2C). This effect was most noticeable with the sub125 μm sieve fraction; however, the large particles in the small-scale reactions generated nearly identical levels of MHET as in the 1 L scale reactions. This suggests that the product released from

https://doi.org/10.1021/acssuschemeng.2c01961
ACS Sustainable Chem. Eng. XXXX, XXX, XXX−XXX

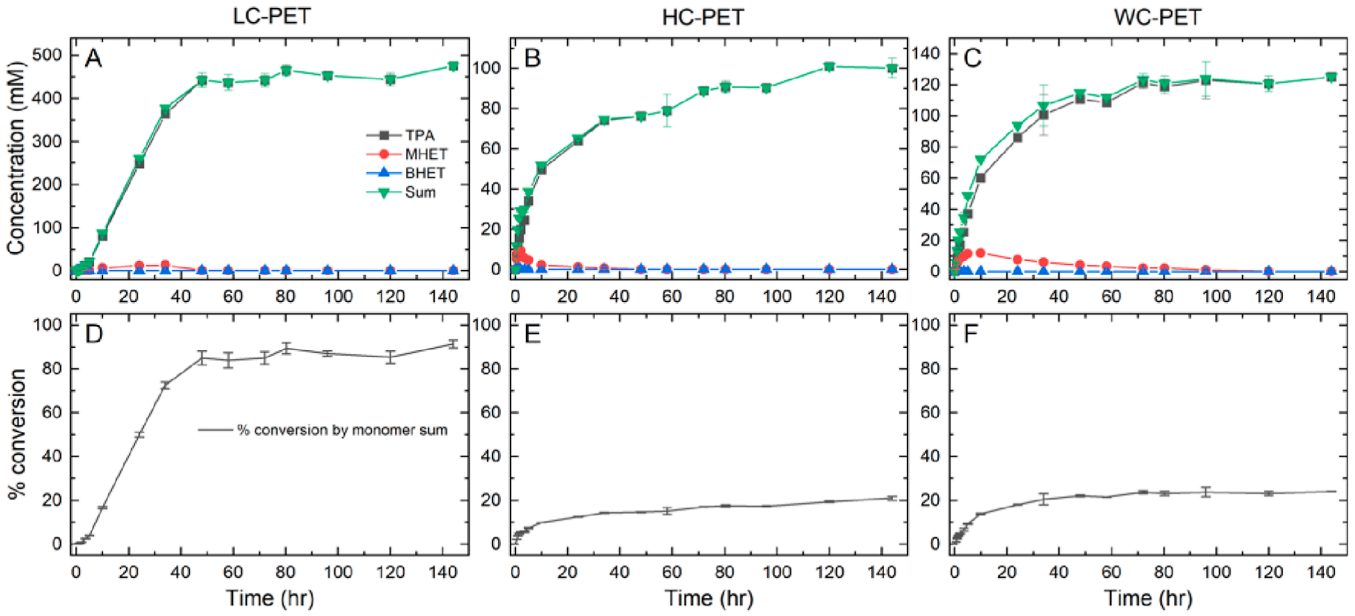

Figure 5. Conversion time courses of 1 L scale reactions conducted in bioreactors. Results from the reaction with various PET substrates at 100 g L^{-1} and 3 mg g^{-1} PET LCC-ICCG enzyme. (A–C) Product release profiles as a function of time measured by HPLC for (A) LC-PET film cut into ~1 × 1 cm squares, (B) HC-PET particles, and (C) WC-PET particles. (D–F) Percent conversion of total PET for (D) LC-PET film cut into ~1 × 1 cm squares, (E) HC-PET particles, and (F) WC-PET particles. Reactions were performed in duplicate, data points show the mean, and error bars show the absolute difference between the duplicates. The data shown in this figure are provided in Dataset S6.

the PET may be affected by surface area or accessibility of the PET chains. Additionally, since the absolute concentrations of MHET are similar across the large-scale and small-scale experiments with the larger particle sizes, it is possible that at this concentration of MHET, the LCC-ICCG enzyme will preferentially release TPA due to product inhibition. This suggests that MHET is inhibitory and raises the possibility that adding a complementary MHETase to the reaction could further improve the performance of LCC-ICCG, as has been shown with a carboxylesterase and WT-LCC,[66] and the *Is*PETase and MHETase system.[22,49]

CONCLUSIONS

Overall, under the conditions tested here, we observe that PET particle size does not have an appreciable effect on the overall degradation performance of LCC-ICCG since each particle size fraction for both substrates reached similar extents of degradation. This is in good agreement with previous work from others that investigated the effect of particle size on enzymatic conversion of PET.[52−54] In these studies, the authors generally concluded that smaller PET particles reached higher levels of conversion over days or weeks. However, the enzymes used in these studies, HiC[52,54] and Thc-Cut1,[53] have been reported to exhibit lower hydrolysis rates and reach substantially lower extents of PET conversion compared to LCC-ICCG.[26,57] This suggests that even for reactions spanning days or weeks, these enzymes could still be working at the initial rate. Stated differently, these previous results suggest that across a variety of enzymes working at different rates and extents of conversion, a reduction in particle size may lead only to an increase in the initial rate of the reaction. While this is certainly beneficial to an industrial process since it would lower the residence time in the reactor, based on TEA analysis, this is not as substantial a cost driver as either extent of depolymerization or the cost associated with generating PET feedstocks.[47] For instance, small amorphous particles (<300 μm, as used by Tournier *et al.*[39]) reach 90% conversion in 10 h. In this study, using the amorphous film cut into small squares, we achieved the same extent of conversion in 48 h (Figure 5). This difference in time would cut the minimum selling price of TPA by less than 6% based on our TEA model. The question then becomes whether the tradeoff in energy consumption (and capital expense) of grinding could be offset by this <6% reduction selling price of TPA—further experiments using LCC-ICCG or other enzymes with various forms of pretreated postconsumer PET waste paired with rigorous TEA will be necessary to determine the efficacy of particle size reduction and amorphization to industrial-scale enzymatic recycling of PET.

ASSOCIATED CONTENT

Supporting Information

The Supporting Information is available free of charge at https://pubs.acs.org/doi/10.1021/acssuschemeng.2c01961.

Additional characterization and kinetic data as well as datasets for all figures (PDF)

AUTHOR INFORMATION

Corresponding Authors

John E. McGeehan − *BOTTLE Consortium, Golden, Colorado 80401, United States; Centre for Enzyme Innovation, School of Biological Sciences, Institute of Biological and Biomedical Sciences, University of Portsmouth, Portsmouth PO1 2DY, U.K.;* orcid.org/0000-0002-6750-1462; Email: john.mcgeehan@port.ac.uk

Gregg T. Beckham − *Renewable Resources and Enabling Sciences Center, National Renewable Energy Laboratory, Golden, Colorado 80401, United States; BOTTLE Consortium, Golden, Colorado 80401, United States;* orcid.org/0000-0002-3480-212X; Email: gregg.beckham@nrel.gov

https://doi.org/10.1021/acssuschemeng.2c01961
ACS Sustainable Chem. Eng. XXXX, XXX, XXX−XXX

Authors

Richard K. Brizendine − *Renewable Resources and Enabling Sciences Center, National Renewable Energy Laboratory, Golden, Colorado 80401, United States; BOTTLE Consortium, Golden, Colorado 80401, United States;* orcid.org/0000-0001-9209-2210

Erika Erickson − *Renewable Resources and Enabling Sciences Center, National Renewable Energy Laboratory, Golden, Colorado 80401, United States; BOTTLE Consortium, Golden, Colorado 80401, United States;* orcid.org/0000-0001-7806-9348

Stefan J. Haugen − *Renewable Resources and Enabling Sciences Center, National Renewable Energy Laboratory, Golden, Colorado 80401, United States*

Kelsey J. Ramirez − *Renewable Resources and Enabling Sciences Center, National Renewable Energy Laboratory, Golden, Colorado 80401, United States; BOTTLE Consortium, Golden, Colorado 80401, United States*

Joel Miscall − *Renewable Resources and Enabling Sciences Center, National Renewable Energy Laboratory, Golden, Colorado 80401, United States; BOTTLE Consortium, Golden, Colorado 80401, United States*

Davinia Salvachúa − *Renewable Resources and Enabling Sciences Center, National Renewable Energy Laboratory, Golden, Colorado 80401, United States*

Andrew R. Pickford − *BOTTLE Consortium, Golden, Colorado 80401, United States; Centre for Enzyme Innovation, School of Biological Sciences, Institute of Biological and Biomedical Sciences, University of Portsmouth, Portsmouth PO1 2DY, U.K.;* orcid.org/0000-0002-7237-0030

Margaret J. Sobkowicz − *Department of Plastics Engineering, University of Massachusetts Lowell, Lowell, Massachusetts 01854, United States;* orcid.org/0000-0003-0571-0952

Complete contact information is available at: https://pubs.acs.org/10.1021/acssuschemeng.2c01961

Author Contributions

G.T.B., J.E.M., and M.J.S. conceived the project and R.K.B. and G.T.B. designed the study. R.K.B. and J.M. characterized the PET substrates, R.K.B. and E.E. expressed and purified the enzyme, and R.K.B. conducted the small-scale depolymerization experiments. R.K.B., E.E., and D.S. conducted the bioreactor experiments. S.J.H. and K.J.R. performed all HPLC analyses. R.K.B. and G.T.B. analyzed the data. The paper was written by R.K.B. and G.T.B. and edited and approved by all authors. G.T.B., J.E.M., A.R.P., and M.J.S. were responsible for funding acquisition.

Notes

The authors declare no competing financial interest.

ACKNOWLEDGMENTS

Funding was provided by the U.S. DOE, Office of Energy Efficiency and Renewable Energy, Advanced Manufacturing Office (AMO) and Bioenergy Technologies Office (BETO) under contract no. DE-FOA-0002029. This work was also performed as part of the Bio-Optimized Technologies to keep Thermoplastics out of Landfills and the Environment (BOTTLE) Consortium and was supported by AMO and BETO under contract no. DE-AC36-08GO28308 with NREL, operated by Alliance for Sustainable Energy, LLC. The BOTTLE Consortium includes members from the University of Portsmouth, funded under contract no. DE-AC36-08GO28308 with NREL and additionally supported by Research England (E3 scheme). The bioreactor experiments were funded by DARPA *via* cooperative agreement number IAG-21-17585. This document was approved by DARPA on January 24, 2022, for public release, distribution unlimited. We thank Western Container Corporation for providing PET fines in support of this work. The views expressed in the article do not necessarily represent the views of the DOE or the U.S. Government. The U.S. Government retains and the publisher by accepting the article for publication, acknowledges that the U.S. Government retains a nonexclusive, paid-up, irrevocable, worldwide license to publish or reproduce the published form of this work, or allow others to do so, for U.S. Government purposes.

REFERENCES

(1) Cózar, A.; Echevarría, F.; González-Gordillo, J. I.; Irigoien, X.; Úbeda, B.; Hernández-León, S.; Palma, Á. T.; Navarro, S.; García-de-Lomas, J.; Ruiz, A.; et al. Plastic debris in the open ocean. *Proc. Natl. Acad. Sci. U.S.A.* **2014**, *111*, 10239−10244.

(2) Jambeck, J. R.; Geyer, R.; Wilcox, C.; Siegler, T. R.; Perryman, M.; Andrady, A.; Narayan, R.; Law, K. L. Marine pollution. Plastic waste inputs from land into the ocean. *Science* **2015**, *347*, 768−771.

(3) Allen, S.; Allen, D.; Phoenix, V. R.; Le Roux, G.; Durántez Jiménez, P.; Simonneau, A.; Binet, S.; Galop, D. Atmospheric transport and deposition of microplastics in a remote mountain catchment. *Nat. Geosci.* **2019**, *12*, 339−344.

(4) Ellis, L. D.; Rorrer, N. A.; Sullivan, K. P.; Otto, M.; McGeehan, J. E.; Román-Leshkov, Y.; Wierckx, N.; Beckham, G. T. Chemical and biological catalysis for plastics recycling and upcycling. *Nat. Catal.* **2021**, *4*, 539−556.

(5) Nicholson, S. R.; Rorrer, N. A.; Carpenter, A. C.; Beckham, G. T. Manufacturing energy and greenhouse gas emissions associated with plastics consumption. *Joule* **2021**, *5*, 673−686.

(6) *PET Polymer: Chemical Economics Handbook*; IHS Markit. https://ihsmarkit.com/products/pet-polymer-chemical-economics-handbook.html (accessed Sept 01, 2021).

(7) Ragaert, K.; Delva, L.; Van Geem, K. Mechanical and chemical recycling of solid plastic waste. *Waste Manage.* **2017**, *69*, 24−58.

(8) Sinha, V.; Patel, M. R.; Patel, J. V. Pet Waste Management by Chemical Recycling: A Review. *J. Polym. Environ.* **2010**, *18*, 8−25.

(9) Wei, R.; Tiso, T.; Bertling, J.; O'Connor, K.; Blank, L. M.; Bornscheuer, U. T. Possibilities and limitations of biotechnological plastic degradation and recycling. *Nat. Catal.* **2020**, *3*, 867−871.

(10) Carniel, A.; Waldow, V. d. A.; Castro, A. M. d. A comprehensive and critical review on key elements to implement enzymatic PET depolymerization for recycling purposes. *Biotechnol. Adv.* **2021**, *52*, 107811.

(11) Wei, R.; Zimmermann, W. Biocatalysis as a green route for recycling the recalcitrant plastic polyethylene terephthalate. *Microbiol. Biotechnol.* **2017**, *10*, 1302−1307.

(12) Müller, R.-J.; Schrader, H.; Profe, J.; Dresler, K.; Deckwer, W.-D. Enzymatic Degradation of Poly(ethylene terephthalate): Rapid Hydrolyse using a Hydrolase from T. fusca. *Macromol. Rapid Commun.* **2005**, *26*, 1400−1405.

(13) Alisch-Mark, M.; Herrmann, A.; Zimmermann, W. Increase of the hydrophilicity of polyethylene terephthalate fibres by hydrolases from *Thermomonospora fusca* and *Fusarium solani* f. sp. *pisi*. *Biotechnol. Lett.* **2006**, *28*, 681−685.

(14) Eberl, A.; Heumann, S.; Brückner, T.; Araujo, R.; Cavaco-Paulo, A.; Kaufmann, F.; Kroutil, W.; Guebitz, G. M. Enzymatic surface hydrolysis of poly(ethylene terephthalate) and bis-(benzoyloxyethyl) terephthalate by lipase and cutinase in the presence of surface active molecules. *J. Biotechnol.* **2009**, *143*, 207−212.

(15) Ronkvist, Å. M.; Xie, W.; Lu, W.; Gross, R. A. Cutinase-Catalyzed Hydrolysis of Poly(ethylene terephthalate). *Macromolecules* **2009**, *42*, 5128−5138.
(16) Ribitsch, D.; Heumann, S.; Trotscha, E.; Herrero Acero, E.; Greimel, K.; Leber, R.; Birner-Gruenberger, R.; Deller, S.; Eiteljoerg, I.; Remler, P.; et al. Hydrolysis of polyethyleneterephthalate by p-nitrobenzylesterase from *Bacillus subtilis*. *Biotechnol. Prog.* **2011**, *27*, 951−960.
(17) Sulaiman, S.; Yamato, S.; Kanaya, E.; Kim, J.-J.; Koga, Y.; Takano, K.; Kanaya, S. Isolation of a novel cutinase homolog with polyethylene terephthalate-degrading activity from leaf-branch compost by using a metagenomic approach. *Appl. Environ. Microbiol.* **2012**, *78*, 1556−1562.
(18) Roth, C.; Wei, R.; Oeser, T.; Then, J.; Föllner, C.; Zimmermann, W.; Sträter, N. Structural and functional studies on a thermostable polyethylene terephthalate degrading hydrolase from *Thermobifida fusca*. *Appl. Microbiol. Biotechnol.* **2014**, *98*, 7815−7823.
(19) Sulaiman, S.; You, D.-J.; Kanaya, E.; Koga, Y.; Kanaya, S. Crystal Structure and Thermodynamic and Kinetic Stability of Metagenome-Derived LC-Cutinase. *Biochemistry* **2014**, *53*, 1858−1869.
(20) Wei, R.; Oeser, T.; Zimmermann, W. Synthetic polyester-hydrolyzing enzymes from thermophilic actinomycetes. *Adv. Appl. Microbiol.* **2014**, *89*, 267−305.
(21) Perz, V.; Bleymaier, K.; Sinkel, C.; Kueper, U.; Bonnekessel, M.; Ribitsch, D.; Guebitz, G. M. Substrate specificities of cutinases on aliphatic-aromatic polyesters and on their model substrates. *New Biotechnol.* **2016**, *33*, 295−304.
(22) Yoshida, S.; Hiraga, K.; Takehana, T.; Taniguchi, I.; Yamaji, H.; Maeda, Y.; Toyohara, K.; Miyamoto, K.; Kimura, Y.; Oda, K. A bacterium that degrades and assimilates poly(ethylene terephthalate). *Science* **2016**, *351*, 1196−1199.
(23) Ribitsch, D.; Hromic, A.; Zitzenbacher, S.; Zartl, B.; Gamerith, C.; Pellis, A.; Jungbauer, A.; Łyskowski, A.; Steinkellner, G.; Gruber, K.; et al. Small cause, large effect: Structural characterization of cutinases from *Thermobifida cellulosilytica*. *Biotechnol. Bioeng.* **2017**, *114*, 2481−2488.
(24) Kawai, F.; Kawabata, T.; Oda, M. Current State and Perspectives Related to the Polyethylene Terephthalate Hydrolases Available for Biorecycling. *ACS Sustainable Chem. Eng.* **2020**, *8*, 8894−8908.
(25) Sonnendecker, C.; Oeser, J.; Richter, P. K.; Hille, P.; Zhao, Z.; Fischer, C.; Lippold, H.; Blazquez-Sanchez, P.; Engelberger, F.; Ramirez-Sarmiento, C. A.; et al. Low Carbon Footprint Recycling of Post-Consumer PET Plastic with a Metagenomic Polyester Hydrolase. *ChemSusChem* **2022**, *15*, No. e202101062.
(26) Herrero Acero, E.; Ribitsch, D.; Dellacher, A.; Zitzenbacher, S.; Marold, A.; Steinkellner, G.; Gruber, K.; Schwab, H.; Guebitz, G. M. Surface engineering of a cutinase from Thermobifida cellulosilytica for improved polyester hydrolysis. *Biotechnol. Bioeng.* **2013**, *110*, 2581−2590.
(27) Ribitsch, D.; Yebra, A. O.; Zitzenbacher, S.; Wu, J.; Nowitsch, S.; Steinkellner, G.; Greimel, K.; Doliska, A.; Oberdorfer, G.; Gruber, C. C.; et al. Fusion of binding domains to *Thermobifida cellulosilytica* cutinase to tune sorption characteristics and enhancing PET hydrolysis. *Biomacromolecules* **2013**, *14*, 1769−1776.
(28) Ribitsch, D.; Herrero Acero, E.; Przylucka, A.; Zitzenbacher, S.; Marold, A.; Gamerith, C.; Tscheliessnig, R.; Jungbauer, A.; Rennhofer, H.; Lichtenegger, H.; et al. Enhanced cutinase-catalyzed hydrolysis of polyethylene terephthalate by covalent fusion to hydrophobins. *Appl. Environ. Microbiol.* **2015**, *81*, 3586−3592.
(29) Then, J.; Wei, R.; Oeser, T.; Barth, M.; Belisário-Ferrari, M. R.; Schmidt, J.; Zimmermann, W. Ca2+ and Mg2+ binding site engineering increases the degradation of polyethylene terephthalate films by polyester hydrolases from *Thermobifida fusca*. *Biotechnol. J.* **2015**, *10*, 592−598.
(30) Wei, R.; Oeser, T.; Schmidt, J.; Meier, R.; Barth, M.; Then, J.; Zimmermann, W. Engineered bacterial polyester hydrolases efficiently degrade polyethylene terephthalate due to relieved product inhibition. *Biotechnol. Bioeng.* **2016**, *113*, 1658−1665.
(31) Shirke, A. N.; Basore, D.; Butterfoss, G. L.; Bonneau, R.; Bystroff, C.; Gross, R. A. Toward rational thermostabilization of *Aspergillus oryzae* cutinase: Insights into catalytic and structural stability. *Proteins* **2016**, *84*, 60−72.
(32) Biundo, A.; Ribitsch, D.; Steinkellner, G.; Gruber, K.; Guebitz, G. M. Polyester hydrolysis is enhanced by a truncated esterase: Less is more. *Biotechnol. J.* **2017**, *12*, DOI: 10.1002/biot.201600450
(33) Shirke, A. N.; Butterfoss, G. L.; Saikia, R.; Basu, A.; Maria, L.; Svendsen, A.; Gross, R. A. Engineered *Humicola insolens* cutinase for efficient cellulose acetate deacetylation. *Biotechnol. J.* **2017**, *12*, 1700188.
(34) Austin, H. P.; Allen, M. D.; Donohoe, B. S.; Rorrer, N. A.; Kearns, F. L.; Silveira, R. L.; Pollard, B. C.; Dominick, G.; Duman, R.; El Omari, K.; et al. Characterization and engineering of a plastic-degrading aromatic polyesterase. *Proc. Natl. Acad. Sci. U.S.A.* **2018**, *115*, E4350−E4357.
(35) Biundo, A.; Ribitsch, D.; Guebitz, G. M. Surface engineering of polyester-degrading enzymes to improve efficiency and tune specificity. *Appl. Microbiol. Biotechnol.* **2018**, *102*, 3551−3559.
(36) Shirke, A. N.; White, C.; Englaender, J. A.; Zwarycz, A.; Butterfoss, G. L.; Linhardt, R. J.; Gross, R. A. Stabilizing Leaf and Branch Compost Cutinase (LCC) with Glycosylation: Mechanism and Effect on PET Hydrolysis. *Biochemistry* **2018**, *57*, 1190−1200.
(37) Son, H. F.; Cho, I. J.; Joo, S.; Seo, H.; Sagong, H.-Y.; Choi, S. Y.; Lee, S. Y.; Kim, K.-J. Rational Protein Engineering of Thermo-Stable PETase from *Ideonella sakaiensis* for Highly Efficient PET Degradation. *ACS Catal.* **2019**, *9*, 3519−3526.
(38) Furukawa, M.; Kawakami, N.; Tomizawa, A.; Miyamoto, K. Efficient Degradation of Poly(ethylene terephthalate) with *Thermobifida fusca* Cutinase Exhibiting Improved Catalytic Activity Generated using Mutagenesis and Additive-based Approaches. *Sci. Rep.* **2019**, *9*, 16038.
(39) Tournier, V.; Topham, C. M.; Gilles, A.; David, B.; Folgoas, C.; Moya-Leclair, E.; Kamionka, E.; Desrousseaux, M.-L.; Texier, H.; Gavalda, S.; et al. An engineered PET depolymerase to break down and recycle plastic bottles. *Nature* **2020**, *580*, 216−219.
(40) Bell, E.; Smithson, R.; Kilbride, S.; Foster, J.; Hardy, F.; Ramachandran, S.; Tedstone, A.; Haigh, S.; Garforth, A.; Day, P.; et al. Directed Evolution of an Efficient and Thermostable PET Depolymerase. *ChemRxiv* **2021**, DOI: 10.26434/chemrxiv-2021-mcjh6.
(41) Cui, Y.; Chen, Y.; Liu, X.; Dong, S.; Tian, Y. e.; Qiao, Y.; Mitra, R.; Han, J.; Li, C.; Han, X.; et al. Computational Redesign of a PETase for Plastic Biodegradation under Ambient Condition by the GRAPE Strategy. *ACS Catal.* **2021**, *11*, 1340−1350.
(42) Nakamura, A.; Kobayashi, N.; Koga, N.; Iino, R. Positive Charge Introduction on the Surface of Thermostabilized PET Hydrolase Facilitates PET Binding and Degradation. *ACS Catal.* **2021**, *11*, 8550−8564.
(43) Guo, B.; Vanga, S. R.; Lopez-Lorenzo, X.; Saenz-Mendez, P.; Ericsson, S. R.; Fang, Y.; Ye, X.; Schriever, K.; Bäckström, E.; Biundo, A.; et al. Conformational Selection in Biocatalytic Plastic Degradation by PETase. *ACS Catal.* **2022**, *12*, 3397−3409.
(44) Lu, H.; Diaz, D. J.; Czarnecki, N. J.; Zhu, C.; Kim, W.; Shroff, R.; Acosta, D. J.; Alexander, B. R.; Cole, H. O.; Zhang, Y.; et al. Machine learning-aided engineering of hydrolases for PET depolymerization. *Nature* **2022**, *604*, 662−667.
(45) Wei, R.; von Haugwitz, G.; Pfaff, L.; Mican, J.; Badenhorst, C. P. S.; Liu, W.; Weber, G.; Austin, H. P.; Bednar, D.; Damborsky, J.; et al. Mechanism-Based Design of Efficient PET Hydrolases. *ACS Catal.* **2022**, *12*, 3382−3396.
(46) Zeng, W.; Li, X.; Yang, Y.; Min, J.; Huang, J.-W.; Liu, W.; Niu, D.; Yang, X.; Han, X.; Zhang, L.; et al. Substrate-Binding Mode of a Thermophilic PET Hydrolase and Engineering the Enzyme to Enhance the Hydrolytic Efficacy. *ACS Catal.* **2022**, *12*, 3033−3040.
(47) Singh, A.; Rorrer, N. A.; Nicholson, S. R.; Erickson, E.; DesVeaux, J. S.; Avelino, A. F. T.; Lamers, P.; Bhatt, A.; Zhang, Y.;

https://doi.org/10.1021/acssuschemeng.2c01961
ACS Sustainable Chem. Eng. XXXX, XXX, XXX−XXX

Avery, G.; et al. Techno-economic, life-cycle, and socioeconomic impact analysis of enzymatic recycling of poly(ethylene terephthalate). *Joule* **2021**, *5*, 2479−2503.
(48) Wei, R.; Breite, D.; Song, C.; Gräsing, D.; Ploss, T.; Hille, P.; Schwerdtfeger, R.; Matysik, J.; Schulze, A.; Zimmermann, W. Biocatalytic Degradation Efficiency of Postconsumer Polyethylene Terephthalate Packaging Determined by Their Polymer Microstructures. *Adv. Sci.* **2019**, *6*, 1900491.
(49) Knott, B. C.; Erickson, E.; Allen, M. D.; Gado, J. E.; Graham, R.; Kearns, F. L.; Pardo, I.; Topuzlu, E.; Anderson, J. J.; Austin, H. P.; et al. Characterization and engineering of a two-enzyme system for plastics depolymerization. *Proc. Natl. Acad. Sci. U.S.A.* **2020**, *117*, 25476−25485.
(50) Erickson, E.; Shakespeare, T. J.; Bratti, F.; Buss, B. L.; Graham, R.; Hawkins, M. A.; König, G.; Michener, W. E.; Miscall, J.; Ramirez, K. J.; et al. Comparative performance of PETase as a function of reaction conditions, substrate properties, and product accumulation. *ChemSusChem* **2022**, *15*, No. e202101932.
(51) Lu, H.; Diaz, D. J.; Czarnecki, N. J.; Zhu, C.; Kim, W.; Shroff, R.; Acosta, D. J.; Alexander, B.; Cole, H.; Zhang, Y. J.; et al. Deep learning redesign of PETase for practical PET degrading applications. *bioRxiv* **2021**, DOI: 10.1101/2021.10.10.463845.
(52) de Castro, A. M.; Carniel, A.; Nicomedes Junior, J.; da Conceição Gomes, A.; Valoni, É. Screening of commercial enzymes for poly(ethylene terephthalate) (PET) hydrolysis and synergy studies on different substrate sources. *J. Ind. Microbiol. Biotechnol.* **2017**, *44*, 835−844.
(53) Gamerith, C.; Zartl, B.; Pellis, A.; Guillamot, F.; Marty, A.; Acero, E. H.; Guebitz, G. M. Enzymatic recovery of polyester building blocks from polymer blends. *Process Biochem.* **2017**, *59*, 58−64.
(54) Castro, A. M. d.; Carniel, A.; Stahelin, D.; Chinelatto Junior, L. S.; Honorato, H. d. A.; de Menezes, S. M. C. High-fold improvement of assorted post-consumer poly(ethylene terephthalate) (PET) packages hydrolysis using Humicola insolens cutinase as a single biocatalyst. *Process Biochem.* **2019**, *81*, 85−91.
(55) Kari, J.; Andersen, M.; Borch, K.; Westh, P. An Inverse Michaelis−Menten Approach for Interfacial Enzyme Kinetics. *ACS Catal.* **2017**, *7*, 4904−4914.
(56) Andersen, M.; Kari, J.; Borch, K.; Westh, P. Michaelis-Menten equation for degradation of insoluble substrate. *Math. Biosci.* **2018**, *296*, 93−97.
(57) Bååth, J. A.; Borch, K.; Jensen, K.; Brask, J.; Westh, P. Comparative Biochemistry of Four Polyester (PET) Hydrolases. *ChemBioChem* **2021**, *22*, 1627−1637.
(58) Werner, A. Z.; Clare, R.; Mand, T. D.; Pardo, I.; Ramirez, K. J.; Haugen, S. J.; Bratti, F.; Dexter, G. N.; Elmore, J. R.; Huenemann, J. D.; et al. Tandem chemical deconstruction and biological upcycling of poly(ethylene terephthalate) to beta-ketoadipic acid by *Pseudomonas putida* KT2440. *Metab. Eng.* **2021**, *67*, 250−261.
(59) Blundell, D. J.; MacKerron, D. H.; Fuller, W.; Mahendrasingam, A.; Martin, C.; Oldman, R. J.; Rule, R. J.; Riekel, C. Characterization of strain-induced crystallization of poly(ethylene terephthalate) at fast draw rates using synchrotron radiation. *Polymer* **1996**, *37*, 3303−3311.
(60) Blundell, D. J.; Mahendrasingam, A.; Martin, C.; Fuller, W.; MacKerron, D. H.; Harvie, J. L.; Oldman, R. J.; Riekel, C. Orientation prior to crystallisation during drawing of poly(ethylene terephthalate). *Polymer* **2000**, *41*, 7793−7802.
(61) Mahendrasingam, A.; Martin, C.; Fuller, W.; Blundell, D. J.; Oldman, R. J.; MacKerron, D. H.; Harvie, J. L.; Riekel, C. Observation of a transient structure prior to strain-induced crystallization in poly(ethylene terephthalate). *Polymer* **2000**, *41*, 1217−1221.
(62) Forestier, E.; Combeaud, C.; Guigo, N.; Sbirrazzuoli, N.; Billon, N. Understanding of strain-induced crystallization developments scenarios for polyesters: Comparison of poly(ethylene furanoate), PEF, and poly(ethylene terephthalate), PET. *Polymer* **2020**, *203*, 122755.
(63) Bashir, Z.; Al-Aloush, I.; Al-Raqibah, I.; Ibrahim, M. Evaluation of three methods for the measurement of crystallinity of PET resins, preforms, and bottles. *Polym. Eng. Sci.* **2000**, *40*, 2442−2455.
(64) Scandola, M.; Focarete, M. L.; Frisoni, G. Simple Kinetic Model for the Heterogeneous Enzymatic Hydrolysis of Natural Poly(3-hydroxybutyrate). *Macromolecules* **1998**, *31*, 3846−3851.
(65) Thomsen, T. B.; Hunt, C. J.; Meyer, A. S. Influence of substrate crystallinity and glass transition temperature on enzymatic degradation of polyethylene terephthalate (PET). *New Biotechnol.* **2022**, *69*, 28−35.
(66) Barth, M.; Honak, A.; Oeser, T.; Wei, R.; Belisário-Ferrari, M. R.; Then, J.; Schmidt, J.; Zimmermann, W. A dual enzyme system composed of a polyester hydrolase and a carboxylesterase enhances the biocatalytic degradation of polyethylene terephthalate films. *Biotechnol. J.* **2016**, *11*, 1082−1087.